LETTER • OPEN ACCESS

# Major moisture shifts in inland Northeast Asia during the last millennium

ENVIRONMENTAL RESEARCH
LETTERS

LETTER

# Major moisture shifts in inland Northeast Asia during the last millennium

**Zhengyu Xia**[1,*], **Wei Yang**[1] **and Zicheng Yu**[1,2,*]

[1] Key Laboratory of Geographical Processes and Ecological Security in Changbai Mountains, Ministry of Education, School of Geographical Sciences, Northeast Normal University, Changchun, People's Republic of China
[2] State Key Laboratory of Black Soils Conservation and Utilization, Northeast Institute of Geography and Agroecology, Chinese Academy of Sciences, Changchun, People's Republic of China
[*] Authors to whom any correspondence should be addressed.

**E-mail:** zhyxia@hotmail.com and yuzc315@nenu.edu.cn

**Keywords:** peatland, *Sphagnum* mosses, paleoenvironmental reconstruction, stable isotopes, Northeast Asia

Supplementary material for this article is available online

OPEN ACCESS

RECEIVED
30 July 2024

REVISED
4 September 2024

ACCEPTED FOR PUBLICATION
16 October 2024

PUBLISHED
25 October 2024



## Abstract

Previous paleoenvironmental data synthesis indicates that arid central Asia ('westerlies Asia') and mid-latitude East Asia ('monsoonal Asia') show anti-phased moisture variations over the last millennium. However, there are very few records from inland Northeast Asia, which obscures the spatial extent of or the boundary between the two domains and hinders the assessment of climate change impacts and consequences across the region. Here, we present a multi-proxy record that combines peat properties, plant macrofossils, and isotopic ratios of *Sphagnum* moss cellulose from a unique precipitation-fed peatland in northern Northeast China to fill this critical data gap. The results show major centennial-scale moisture anomalies at this site, with drier and wetter conditions during the Medieval Warm Period and Little Ice Age, respectively, which resemble the pattern of moisture changes in 'westerlies Asia'. During the period of rapid anthropogenic warming, the site is much drier, with isotopic evidence for threshold-like summer desiccation of peat-forming *Sphagnum* mosses. This study provides the long-term context and identifies the large-scale pattern of moisture variability in an inland region home to carbon-rich peatlands, forests, and permafrost soils, and highlights their potential vulnerability to future warming-enhanced drying that can be transmitted widely through atmospheric teleconnection.

## 1. Introduction

The spatial patterns and driving mechanisms of moisture variability during past warm and cold periods are of great scientific interest due to their relevance in predicting future continental moisture availability under anthropogenic global warming [1–5]. These are crucial for informing water resource management, ecosystem preservation, and the development of adaptation and mitigation strategies [6–11]. To this end, our current knowledge largely relies on paleoenvironmental records from various natural archives, as Earth system models are uncertain in simulating precipitation or soil moisture dynamics, and instrumental data are typically too short in length [5, 12–14].

There are many high-quality paleoenvironmental records in Asia which, from data syntheses, have already revealed intriguing out-of-phase or anti-phased moisture anomalies among geographically adjacent regions over multiple timescales [15–18]. During the last millennium, previous studies have shown that arid central Asia was drier during the Medieval Warm Period (MWP) than during the Little Ice Age (LIA), whereas mid-latitude East Asia had changes in the opposite direction [4, 15]. These two domains are now referred to as 'westerlies Asia' and 'monsoonal Asia', respectively, to highlight the dominant role of large-scale atmospheric circulation systems in producing spatially inconsistent moisture variations [4].

Despite the significant progress to date, there is still an outstanding data gap from inland Northeast Asia, located at the northeastern end of the presumed boundary between these two domains (figure 1(b)) [19]. While tree-ring records provide insights into

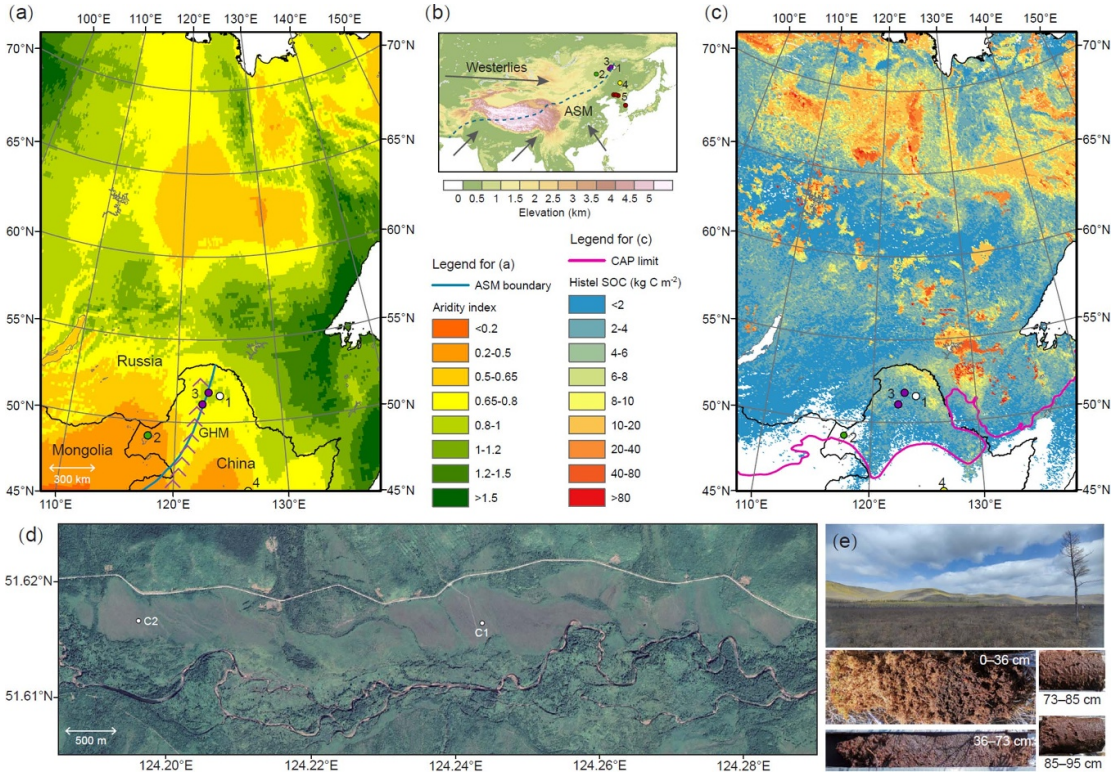


**Figure 1.** Overview of the study region and site. (a) Map of the multi-year aridity index (precipitation divided by potential evapotranspiration) from the CRU (Climatic Research Unit) dataset [35], where drylands are defined as areas with an aridity index of $<0.65$. The blue line indicates the presumed modern boundary of the Asian summer monsoon (ASM) as in [4], which regionally traces the range of the Greater Hinggan Mountains (GHM). (b) The geographical setting of our study site, including continental topography and the same modern boundary of the ASM (dashed blue line) tentatively separating the 'westerlies Asia' and 'monsoonal Asia' domains. (c) Map of histel (permafrost peatland) soil organic carbon (SOC) storage from [36]. The pink line traces the southernmost limit of the circum-Arctic permafrost (CAP) area from [37]. In maps (a)–(c), dots indicate the locations of relevant sites discussed in this paper: 1–Hongtu peatland (this study), 2–Hulun Lake [38], 3–two pine tree-ring sampling sites [39], 4–Harbin City, 5–four Northeast Asia speleothems [26]. (d) Google Earth aerial image of Hongtu peatland (August 2019) marked with the coring locations of HT22-C1 and HT22-C2. (e) Author photos of peatland site and core HT22-C1.

historical drought patterns, most of these records were collected from westerlies-affected Mongolian drylands or cover only several centuries [20–25]. Other studies have developed paleoenvironmental records from monsoon-affected, temperate Northeast China, which do not necessarily represent our study region [26–30], or relied on interpretations of ambiguous proxies such as pollen assemblages and wildfire events that likely have complex responses to temperature and moisture changes [31–34]. Consequently, it remains unclear whether this region is more dynamically linked to mid-latitude westerlies or the Asian summer monsoon (ASM).

As a geographically extensive and sparsely populated region, we note that 'inland Northeast Asia' is actually a rarely used term in current literature and should include northern Northeast China, eastern Mongolia, and parts of Russian Siberia (see an informal map from figure S1 [40]). This region, perhaps little known to other parts of the world, features a mosaic of low-elevation dryland and high-elevation non-dryland areas (figure 1(a)), with considerable forest biomass and peatland coverage underlain by permafrost and frequently affected by wildfire events (figure 1(c)) [36, 41–44]. In the context of rapid anthropogenic warming, these carbon-rich ecosystems are likely highly sensitive to warming-driven changes in the water cycle, including dryland expansion [45, 46], regime shifts in soil moisture dynamics [20, 47, 48], and permafrost thaw [36, 49]. However, the lack of knowledge about how long-term moisture availability responds to temperature variability in this region complicates assessments of climate change impacts on terrestrial ecosystems, including carbon-cycle feedbacks, and projections of their future trajectories.

To address this gap, we present a multi-proxy paleoenvironmental record spanning more than the past two millennia based on a unique, moisture-sensitive peatland within the inland Northeast Asia region. Our new record constrains the centennial-scale temperature-moisture relationship, presents novel evidence that the recent intensification of warm–dry condition has already caused unprecedented shifts in peatland ecosystems, and provides insights into the future vulnerability of terrestrial ecosystems.

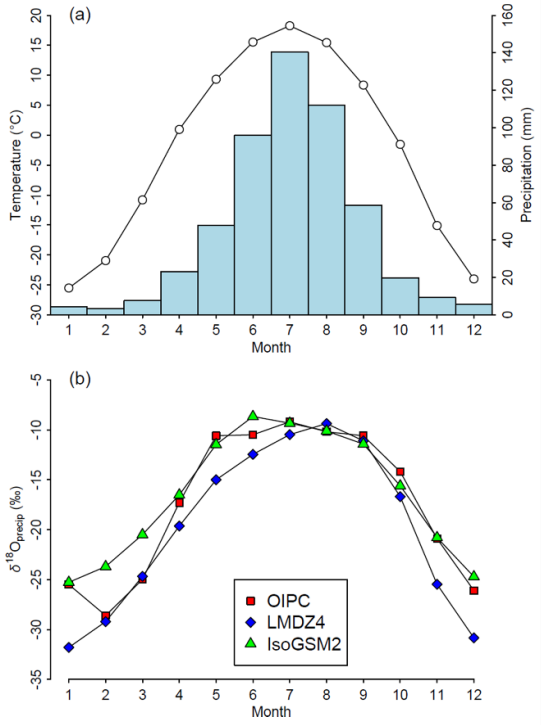


**Figure 2.** (a) Twelve-monthly mean temperature (line with dots) and precipitation (bars) from Xinlin station (1972–2022 CE). (b) Twelve-monthly mean precipitation $\delta^{18}O$ at Hongtu peatland estimated from the observation-based Online Isotopes in Precipitation Calculator (OIPC) [52] and two nudged isotope-enabled general circulation models (GCMs) LMDZ4 [53] and IsoGSM2 [54] during 1979–2021 CE.

## 2. Materials and methods

The study site, Hongtu peatland (51.6° N, 124.2° E; elevation 550 m asl), is located on the eastern side of the Greater Hinggan Mountains in northern Northeast China (figure 1(a)). The mean annual temperature is −2.5 °C and the mean annual precipitation is 528 mm based on instrumental data (1972–2022 CE) from Xinlin station, about 15 km away (figure 2(a)). The peatland vegetation is dominated by *Sphagnum* mosses (mostly nutrient-poor species such as *S. magellanicum*), along with *Polytrichum* mosses and other trees, shrubs, and sedges commonly found in regional peatlands [50]. The peatland is underlain by ice-poor permafrost that separates the site from the mineral-rich groundwater. The field-measured pore-water pH is about 4.4, and electrical conductivity is <20 $\mu$S cm$^{-1}$, confirming that this site mainly relies on a meteoric source of moisture [51]. To our knowledge, Hongtu peatland is a rarely reported site in China for its precipitation-fed nature and long history of *Sphagnum* peat accumulation.

We collected two peat cores in September 2022: HT22-C1 (95 cm) from the central part and HT22-C2 (65 cm) from the western part (figure 1(d)). HT22-C1 contains a 22-cm frozen peat section in the permafrost collected using a drilling machine (figure 1(e)). These two cores did not reach the permafrost basal peat due to machine failure. Back in the laboratory, the cores were sliced and then analyzed to collect a routine suite of paleoecological data, following well-established protocols for each type of analysis.

Radiocarbon dates were measured at seven horizons for each core and then input to the Bacon program for developing age-depth models [55]. Physical properties of peat were determined at every 1 cm using the loss-on-ignition analysis [56]. The derived organic matter (OM) content and ash-free bulk density (AFBD) have been used as qualitative indicators for the degree of decomposition and thus moisture conditions in peat-core studies [57, 58]. Apparent carbon accumulation rates, which may further detect short-term intervals of enhanced peat decomposition, were calculated between dated intervals based on the age-depth model, AFBD, and assumed carbon content of 50% [59, 60].

Simple plant macrofossil types, including *Sphagnum*, *Polytrichum*, herbaceous, ligneous, and charcoal remains, were identified under a stereo microscope at every 1 cm for HT22-C1 and every 2 cm for HT22-C2 [58, 61]. In each sample, at least 20 views were examined to calculate the average volume percentages of macrofossil types. *Sphagnum* moss macrofossils were also identified to the section level from at least 60 random individual leaves under a compound microscope (other studies count at least 100; e.g. [62]). Depending on the objectives of different studies, plant macrofossils have been used to infer changes in peatland vegetation and thus successional processes [63, 64], or reconstruct changes in moisture conditions using statistical techniques [65, 66].

Carbon and oxygen isotopic compositions of *Sphagnum* stem cellulose (extracted following the laboratory method by [67–69]) were analyzed at every 1 cm, except for a few horizons with insufficient preserved stem macrofossils, using an elemental analyzer–isotope ratio mass spectrometer coupled system (Thermo Fisher Scientific Flash 2000 HT–MAT253) housed at the Northeast Institute of Geography and Agroecology, Chinese Academy of Sciences. The typical analytical precision is 0.15‰ for $\delta^{13}C$ and 0.2‰ for $\delta^{18}O$. Recent studies suggest that *Sphagnum* cellulose $\delta^{13}C$ ($\delta^{13}C_{cell}$) and $\delta^{18}O$ ($\delta^{18}O_{cell}$) are potentially powerful paleoenvironmental proxies from peatland archives, in particular when interpreting $\delta^{13}C_{cell}$ and $\delta^{18}O_{cell}$ data as a pair [67, 70]. Specifically, *Sphagnum* $\delta^{13}C_{cell}$ has been used as a moisture indicator [71, 72], and *Sphagnum* $\delta^{18}O_{cell}$ has been interpreted as a proxy for precipitation $\delta^{18}O$ ($\delta^{18}O_{precip}$) that contains composite climate signatures [67, 73].

We combine the above multi-proxy data to interpret past shifts in moisture conditions, focusing on three centennial-scale climate intervals with previously established, regionally suitable time frames [4, 15]: MWP (1000–1300 CE), LIA (1400–1900 CE), and the current warm period (CWP; since 1900 CE).

**Table 1.** Summary of radiocarbon data. Post-bomb dates are reported in italics.

| Dated depth (cm) | Lab number | Dated material | $\delta^{13}C$ (‰) | $^{14}C$ age ($^{14}C$ year BP $\pm$ 1$\sigma$) for pre-bomb date or *'Fraction Modern' ($F^{14}C \pm 1\sigma$)* for post-bomb date | Calibrated age range (cal. year BP, 2$\sigma$) for pre-bomb date or *two possible ages (CE)* for post-bomb date |
|---|---|---|---|---|---|
| **HT22-C1** | | | | | |
| 11–12 | UCIAMS-281047[a] | *Sphagnum* stems/leaves | | *1.0385 ± 0.0016* | *1956, 2011–2013*[c] |
| 18–19 | Beta-683312[b] | *Sphagnum* stems/leaves | –28.7 | *1.0406 ± 0.0039* | *1956*[c], *2010–2013* |
| 25–26 | UCIAMS-281048 | *Sphagnum* stems/leaves | | 75 ± 15 | 255–226, 140–112, 73–35 |
| 38–39 | UCIAMS-281049 | *Sphagnum* stems/leaves | | 75 ± 15 | 255–226, 140–112, 73–35 |
| 54–55 | UCIAMS-281050 | *Sphagnum* stems/leaves | | 320 ± 15 | 450–351, 335–310 |
| 68–69 | UCIAMS-281051 | *Sphagnum* stems/leaves | | 830 ± 15 | 772–760, 745–686 |
| 90–91 | UCIAMS-281052 | *Sphagnum* stems/leaves | | 1455 ± 15 | 1365–1305 |
| **HT22-C2** | | | | | |
| 14–15 | UCIAMS-281053 | *Sphagnum* stems/leaves | | *1.0223 ± 0.0026* | *1955–1956, 2013–2017*[c] |
| 20–21 | Beta-683313 | *Sphagnum* stems/leaves | –26.9 | *1.3332 ± 0.0050* | 1962[d], *1976–1978*[c] |
| 27–28 | UCIAMS-289313 | *Sphagnum* stems/leaves | | *1.0016 ± 0.0015* | *1954–1955*[c], 2019 |
| 34–35 | UCIAMS-281054 | *Sphagnum* stems/leaves | | 30 ± 15 | 246–229, 135–116, 60–42 |
| 43–44 | Beta-683314 | *Sphagnum* stems/leaves | –28.1 | 1550 ± 30 | 1520–1363 |
| 49–50 | UCIAMS-281055 | *Sphagnum* stems/leaves | | 1780 ± 15 | 1715–1691, 1671–1619 |
| 62–63 | UCIAMS-281056 | *Sphagnum* stems/leaves | | 2515 ± 15 | 2724–2695, 2639–2613, 2594–2499 |

[a] UCIAMS: Analysis completed at the Keck-CCAMS Laboratory at the University of California, Irvine, USA.

[b] Beta: Analysis completed at the Beta Analytic Testing Laboratory, Miami, USA.

[c] Selected post-bomb ages.

[d] This age is much less likely than the other based on the general relationship between cumulative peat mass and peat age [75, 76].

## 3. Results

Radiocarbon dates and age-depth models are presented in table 1 and figure 3. Briefly, both cores contain multiple post-bomb (after 1950 CE) dates that anchor the chronology for near-surface peat [74]. HT22-C1 dates back to about 1400 years before present (present is 1950 CE) with stable peat accumulation rates. The relatively shorter HT22-C2 dates further back to about 2700 years before present, with a long interval of very slow peat accumulation at 27–35 cm depth. Its chronology is well-constrained before 1400 years BP and after 1950 CE but is poorly resolved during the MWP and LIA. As such, time series of peat-core data from HT22-C2 should be interpreted with extreme caution for this interval. Fortunately, concatenating the data from two cores still allows us to obtain a continuous proxy dataset spanning the past 2700 years.

The OM content averages 90% in both cores (figure S2), indicating pure peat accumulation without any mineral-rich layers. For HT22-C1, the AFBD averages 0.08 g $cm^{-3}$, generally increasing with depth due to decomposition and compaction (figure S2(a)). The long-term apparent carbon accumulation rate is about 27.7 g C $m^{-2}$ $yr^{-1}$. There is a distinct layer of high AFBD and low OM content at 15–20 cm depth (figure S2(a)). However, we cannot confidently constrain the chronology of that layer because its bottom has a pre-bomb age that ranges by more than 200 years after calibration (UCIAMS-281048; table 1). For HT22-C2, the AFBD averages 0.1 g $cm^{-3}$ and is highest, about 0.2 g $cm^{-3}$, at the section of slow peat accumulation (figure S2(b)). The long-term apparent carbon accumulation rate is about 11.8 g C $m^{-2}$ $yr^{-1}$. A similar distinct layer of high AFBD and low OM content is also present at 16–19 cm depth (figure S2(b)). Importantly, this layer

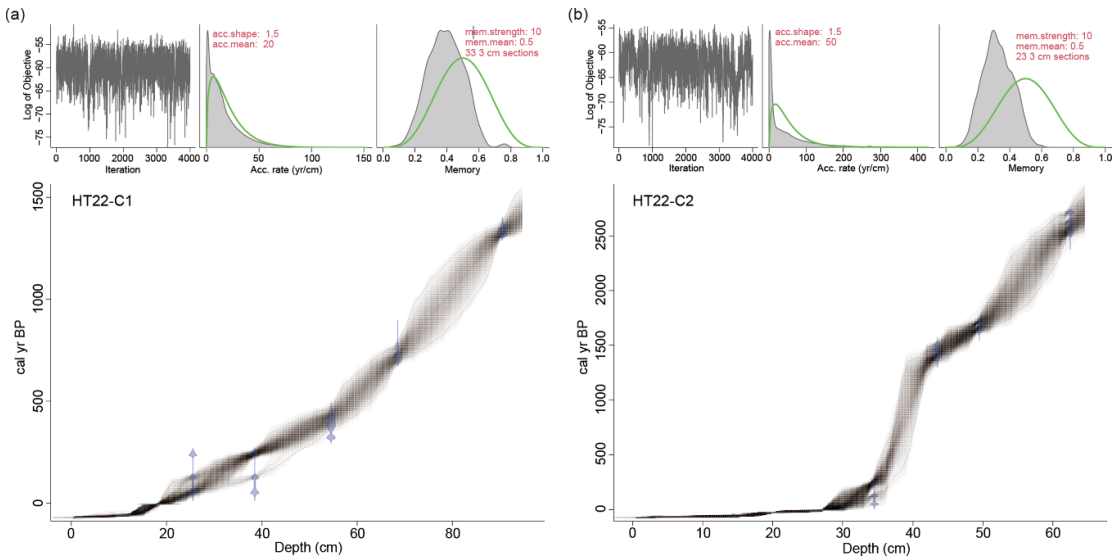


**Figure 3.** Age-depth models of cores (a) HT22-C1 and (b) HT22-C2, generated from the Bacon program [55]. The section thickness (*thick*) was set to 3 cm, and other prior parameters were set to default.

has a precisely constrained chronology by two post-bomb dates, showing a clearly decreased carbon accumulation rate superimposed on the increasing trend toward the core top, where peat has experienced a shorter time of aerobic decomposition (figure S3(b)) [75, 77, 78].

Macrofossil data indicate that the botanical composition of peat is dominated by *Sphagnum* moss fragments throughout both cores (averaged at a volume ratio of >60%), specifically by *S.* section *Sphagnum* such as *S. magellanicum* (figure S2). The rest of the material is mostly fragments from herbaceous and ligneous vegetation types (figure S2). However, we did not identify these vascular plant macrofossils to the species level. *Polytrichum* moss (*Polytrichum* cf. *strictum/commune*) fragments commonly found in very dry peatland habitats and charcoal are of minor importance (figure S2). However, these are perhaps the most straightforward macrofossil types as moisture indicators. Their abundances show notable variations in both cores, being relatively abundant in some intervals and absent in others (figure 4(d)).

*Sphagnum* $\delta^{13}$C values, after a simple 'Suess effect' correction (following the method by [80]), range from −30.8‰ to −27.0‰ in HT22-C1 and from −29.6‰ to −25.7‰ in HT22-C2 (figure 4(c)). There are minor centennial-scale variations during the last millennium in well-dated HT22-C1, and shifts of much larger magnitude to lower $\delta^{13}C_{cell}$ values during the CWP in both cores (figures 4(c) and 5(e)). *Sphagnum* $\delta^{18}O_{cell}$ values show large variations, from 12.5‰ to 19.3‰ in HT22-C1 and from 13.3‰ to 19.4‰ in HT22-C2 (figure 4(a)). There are major shifts to lower $\delta^{18}O_{cell}$ values during the LIA in well-dated HT22-C1 and during the CWP in both cores (figures 4(a) and 5(c)).

## 4. Discussion

### 4.1. Moisture changes before the CWP

It has been well established that *Sphagnum* $\delta^{13}C_{cell}$ is a proxy for local *Sphagnum* wetness [70, 82–84]. Our $\delta^{13}C_{cell}$ data indicate small-magnitude shifts (1‰) to drier conditions (lower $\delta^{13}C_{cell}$ values) during the MWP as well as the earlier Sui-Tang Warm Period (STWP; 541-760 CE) of China [85, 86], and slightly wetter conditions (higher $\delta^{13}C_{cell}$ values) during the LIA (figure 4(c)). Compared to previous studies that undertook the same type of proxy analysis (using *Sphagnum* stem materials) [67, 71, 72, 87], our record is unique for its persistently low values of $\delta^{13}C_{cell}$, close to the driest end (about −29‰; after the 2‰ 'Suess effect' correction) found in modern *Sphagnum* mosses [70]. Therefore, it is likely that the $\delta^{13}C_{cell}$ proxy from such dry sites has limited sensitivity to past shifts toward further drier conditions. Nevertheless, our interpretations of moisture changes are supported by plant macrofossil data. The abundances of dry-adapted *Polytrichum* mosses and wildfire-produced charcoal fragments increase from the STWP, remain high during the MWP, and decrease to complete disappearance during the LIA (figure 4(d)). These changes are highly coherent with the pollen-based quantitative precipitation reconstruction from Hulun Lake located in the dryland region west of the Greater Hinggan Mountains (figures 1(a)–(c) and 4(d)) [38], which is one of the very few late-Holocene paleoenvironmental records close enough to our site for a comparison.

Previous studies suggest that *Sphagnum* $\delta^{18}O_{cell}$ is a proxy for $\delta^{18}O_{precip}$ in precipitation-fed peatlands [73, 88]. The $\delta^{18}O_{precip}$ signal is transferred into plant tissues following a simple model:

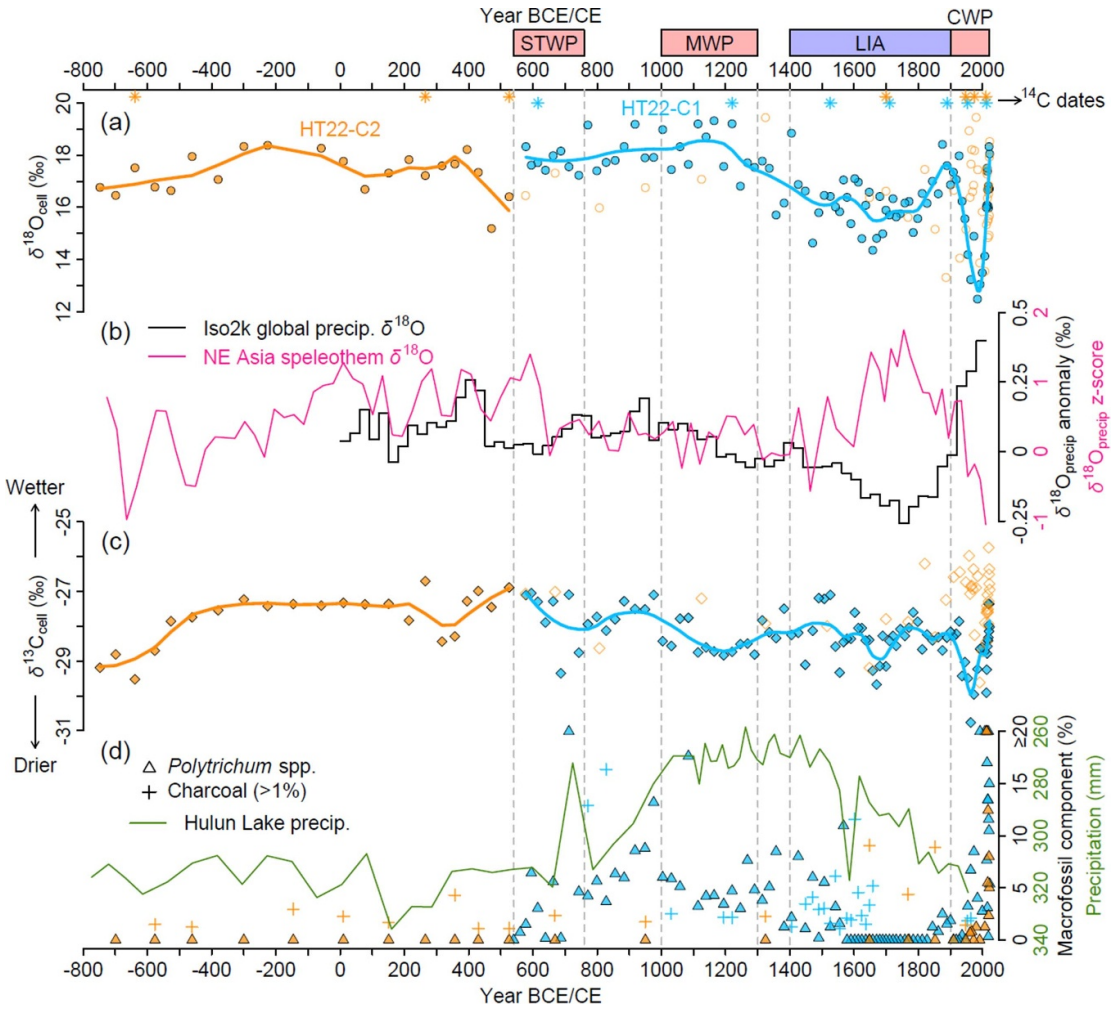


**Figure 4.** Hongtu peatland-based paleoenvironmental record over the past 2800 years. (a) *Sphagnum* $\delta^{18}O_{cell}$ from two cores along with their LOESS (locally estimated scatterplot smoothing) curves. The data from HT22-C2 that temporally overlap with HT22-C1 are plotted as open dots (without LOESS). Asterisks indicate $^{14}C$ dating horizons in two cores. (b) Global median $\delta^{18}O_{precip}$ anomaly from the Iso2k database [79] and Northeast Asia composite $\delta^{18}O_{precip}$ *z*-score based on four speleothem sites from temperate Northeast China and South Korea (figure 1(b)) [26]. (c) Similar to (a), but for 'Suess effect'-corrected *Sphagnum* $\delta^{13}C_{cell}$. (d) *Polytrichum* spp. and charcoal (plotted if more than 1%) percentages from two cores. Also shown is the pollen-based precipitation reconstruction (inverted scale) from Hulun Lake (figures 1(a)–(c)) [38]. Top horizontal bars and dashed lines through subplots correspond to major climate intervals mentioned in the main text.

$\delta^{18}O_{cell} = \delta^{18}O_{precip} + \Delta + \varepsilon$ [82, 89], where $\Delta$ represents a small leaf water evaporation (about 0–3‰) [89], and $\varepsilon$ represents the biochemical fractionation (27‰) [90]. Prior to the CWP, the major shift (>2‰) to lower $\delta^{18}O_{cell}$ values during the LIA after a long period of relatively higher values is highly similar to the long-term trend in global $\delta^{18}O_{precip}$ extracted from the newly available Iso2k database (figures 4(a) and (b)), the latter of which has been interpreted as reflecting temperature-driven global water cycle changes [79]. From this coherent pattern indicative of a common driver and the regional dominance of the isotopic 'temperature effect'—the positive correlation between temperature and $\delta^{18}O_{precip}$ (figure 2) [91], we infer that our $\delta^{18}O_{cell}$ data mainly reflect temperature-related changes in mean-state $\delta^{18}O_{precip}$ during this period, whereas other changes, such as the degree of evaporative enrichment ($\Delta$) and growing-season productivity (affecting the seasonal bias in $\delta^{18}O_{cell}$; text S1), may play a secondary role or contribute to amplifying the magnitude of the LIA shift. Importantly, the lower $\delta^{18}O_{precip}$ during the LIA in our record contrasts with higher $\delta^{18}O_{precip}$ reconstructed from multiple speleothem records from temperate Northeast China and South Korea (figures 1(b) and 4(b)) [26], or even from subtropical China [92]. These speleothem-based studies have linked higher $\delta^{18}O_{precip}$ with lower ASM intensity or rainfall [26, 93], that is, a drier condition during the LIA in northern China (including temperate Northeast China) [4, 15]. This anti-phased $\delta^{18}O_{precip}$ shift indicates that our study region was not directly affected by large-scale temporal ASM dynamics, potentially due to different moisture sources from 'monsoonal Asia'.

Together, our new data document centennial-scale moisture shifts closely linked to natural temperature variability before the CWP, with warm–dry and

cold–wet patterns that are likely persistent features over inland Northeast Asia. This finding provides an important constraint on large-scale spatiotemporal climate patterns over Asia, which will be discussed in section 4.3.

### 4.2. Drier conditions and summer desiccation of *Sphagnum* mosses during the CWP

Our *Sphagnum* $\delta^{13}C_{cell}$ and $\delta^{18}O_{cell}$ data show dramatic and coupled shifts with an unprecedented rate and amplitude during the CWP (figures 4(a) and (c)). Specifically, $\delta^{13}C_{cell}$ values are lower by about 3‰ and $\delta^{18}O_{cell}$ values are lower by about 6‰ during 1940–2010 CE in HT22-C1, before returning to their pre-shift levels after 2010 CE (figures 5(c) and (e)). There are similar shifts of $\delta^{13}C_{cell}$ and $\delta^{18}O_{cell}$ in terms of the magnitude and temporal structure, but showing a different time span of 1990–2010 CE (figures 5(c) and (e)). Although we are confident that shifts to lower $\delta^{13}C$ values indicate drier conditions, the rapid (decades-long), large-magnitude, negative (to lower values) $\delta^{18}O$ excursions shown in our record are quite puzzling. To our knowledge, such recent $\delta^{18}O$ excursions are rarely found in other high-resolution $\delta^{18}O_{precip}$ records in Asia or even globally, which are mostly developed from speleothem archives [2, 92, 94, 95]. If we still adopt the aforementioned interpretive framework attributing such shifts to temperature-related changes in mean-state $\delta^{18}O_{precip}$, these data would suggest strong 'cooling events', which are refuted by multiple lines of evidence.

First, instrumental climate data, including that from the >140 year-long Harbin station (figures 1(a)–(c)) [81], show a gradually increasing trend in temperature throughout the CWP (figure 5(a)). Second, centuries-long tree-ring $\delta^{18}O_{cell}$ records from the same region do not contain the multi-decadal variability comparable to our $\delta^{18}O_{cell}$ data (figure 5(d)) [39], which we would expect to see if there were a major shift in $\delta^{18}O_{precip}$ linked to large-scale atmospheric transition. Additionally, isotope-enabled general circulation models (GCMs) [53, 54] nudged by reanalysis products do not simulate any such variability in $\delta^{18}O_{precip}$ over the recent four decades (figure 5(d)). Third, it is important to note again that the shifts to lower $\delta^{18}O_{cell}$ values are asynchronous between the two cores but are synchronous with large-magnitude shifts to lower $\delta^{13}C_{cell}$ values in the respective cores, meaning that the phenomenon is highly likely related to local moisture dynamics (figures 5(c) and (e)). There is a statistically significant positive correlation between $\delta^{18}O_{cell}$ and $\delta^{13}C_{cell}$ data from HT22-C1 since 1850 CE, owing to their highly similar temporal structure and long duration of shifts (figure 5(g)). Therefore, we need to consider a previously unrecognized, novel mechanism that can reconcile three outstanding characteristics of $\delta^{18}O_{cell}$ data during this period: (i) large magnitude, (ii) tight coupling with $\delta^{13}C_{cell}$, and (iii) asynchrony in different cores.

Here, we propose that such dramatic and coupled shifts to very low $\delta^{18}O_{cell}$ and $\delta^{13}C_{cell}$ values may result from a strongly altered seasonal distribution of *Sphagnum* moss growth. This mechanism is first based on the observation that our study region has a very large $\delta^{18}O_{precip}$ seasonality, with higher summer values and lower winter values differing by up to 20‰ controlled by the same large temperature seasonality (figure 2) [91]. Therefore, any subtle decrease in biomass production during the summer and—in turn—the relatively increased proportion of biomass production using cold-season precipitation such as the snowmelt during the earliest growing season, would theoretically be sufficient to fingerprint much lower $\delta^{18}O_{cell}$ signals even without a notable change in mean-state $\delta^{18}O_{precip}$ [73, 96].

Second, this mechanism aligns with our understanding of plant physiology built in the literature. For example, laboratory-based flux measurements show that the photosynthesis of *Sphagnum* mosses is highly sensitive to moisture availability, slowing down steeply with decreasing water content without immediate recovery after rewetting (or intermittent precipitation events) [83, 97, 98]. Field-based growth measurements also support that *Sphagnum* mosses have an extended growing season compared to vascular plants [99–101], with some studies showing concentrated growth in spring and autumn due to seasonally high surface wetness [102, 103], whereas summer growth can be substantially reduced in drier years due to enhanced moisture limitation [104, 105].

Applying this interpretive framework, we can use simple isotopic mass balance with modern end-members of summer (June–August) and cold-season (November–March) $\delta^{18}O_{precip}$ to quantify the changing nature of *Sphagnum* growth that can explain the observed magnitude of $\delta^{18}O_{cell}$ variability during this period (figure 5(h) and text S1). We estimate that the relative proportion of summer-to-annual *Sphagnum* biomass production has varied from >79% to 17%–65% in HT22-C1 and from >89% to 26%–73% in HT22-C2, with exact values dependent on the type of $\delta^{18}O_{precip}$ inputs and the actual magnitude of evaporative enrichment (figure 5(h) and text S1). We interpret these pronounced reductions in summer growth concurrent with much lower $\delta^{13}C_{cell}$ as reflecting possible decades of summer desiccation for *Sphagnum* mosses under extremely low surface wetness.

We find that this interpretation is strongly supported by our multi-proxy data. For example, the high-AFBD, low-OM content layers temporally coincide with observed isotopic shifts in both cores (figure 5(f)), indicating enhanced peat decomposition during the period of summer desiccation. For

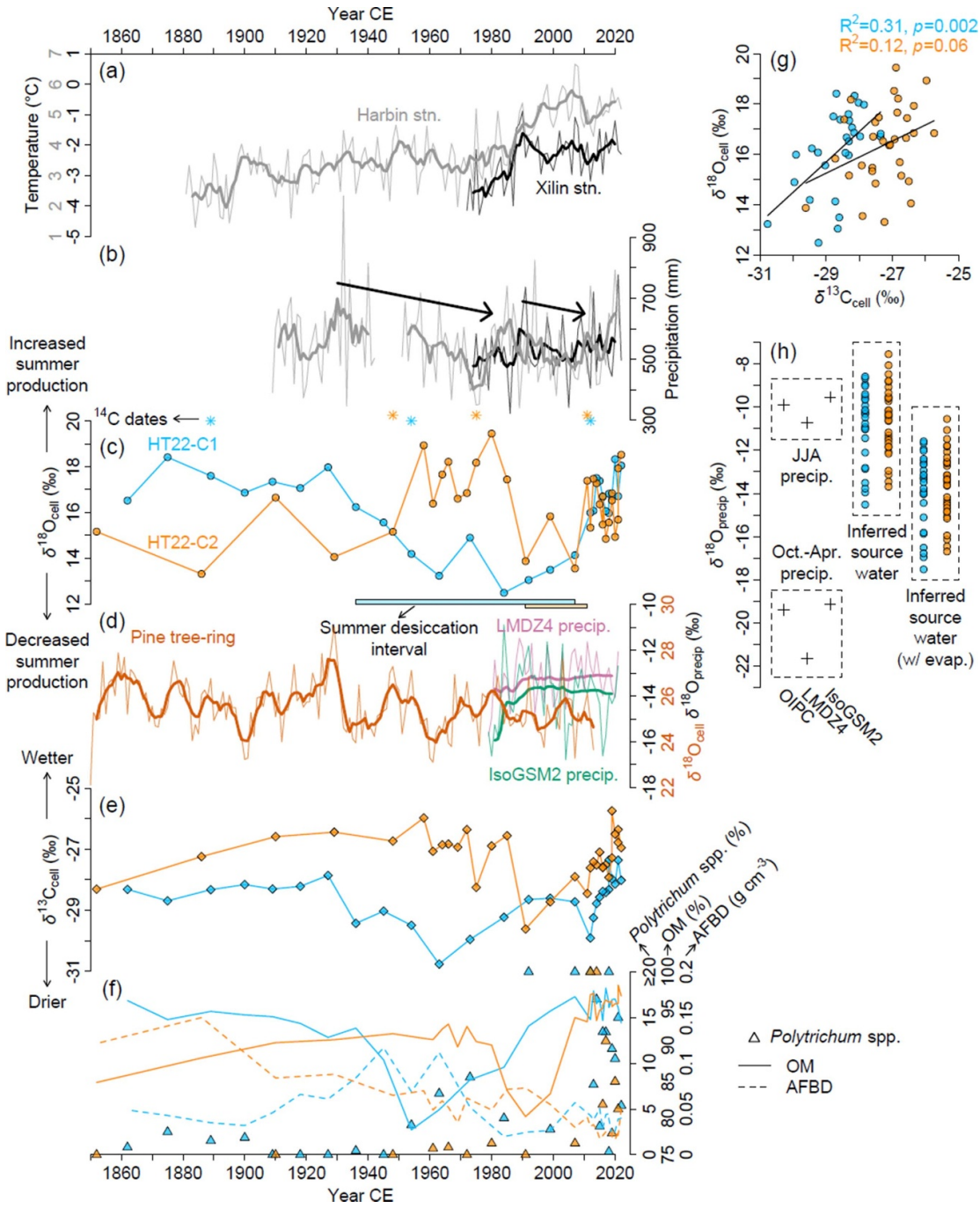


**Figure 5.** Response of Hongtu peatland to the anthropogenic warming. (a) Annual temperature record from the >140-year-long Harbin station (figures 1(a)–(c)) [81] and the local Xinlin station with their 5-year averages (thick lines). (b) Similar to (a), but for annual precipitation, in which two relevant periods of decreasing precipitation are highlighted. (c) *Sphagnum* $\delta^{18}O_{cell}$ from two cores. Asterisks indicate their $^{14}C$ dating horizons. Horizontal bars correspond to the inferred periods of summer desiccation for *Sphagnum* mosses. (d) Mongolian pine (*Pinus sylvestris* var. *mongolica*) $\delta^{18}O_{cell}$ record from the Greater Hinggan Mountains (figures 1(a)–(c)) [39] and amount-weighted mean annual $\delta^{18}O_{precip}$ at Hongtu peatland simulated from two nudged isotope-enabled GCMs LMDZ4 [53] and IsoGSM2 [54] during 1979–2021 CE, along with their 5 year averages (thick lines). (e) Similar to (c), but for 'Suess effect'-corrected *Sphagnum* $\delta^{13}C_{cell}$. (f) *Polytrichum* spp. macrofossil percentage, OM content, and AFBD from two cores. (g) Scatter plot and correlation statistics between *Sphagnum* $\delta^{18}O_{cell}$ and corrected $\delta^{13}C_{cell}$ data from two cores since 1850 CE. (h) Amount-weighted summer (June–August) and cold-season (October–April) $\delta^{18}O_{precip}$ at Hongtu peatland, estimated from the Online Isotopes in Precipitation Calculator (OIPC) [52] and two GCMs (LMDZ4 and IsoGSM2), are compared with the ranges of inferred *Sphagnum* moss source water $\delta^{18}O$ of two cores (since 1850 CE) assuming no or maximum (3‰) evaporative enrichment effect (text S1).

HT22-C2, this layer has a tightly constrained chronology and further shows decreased carbon accumulation rates, supporting impaired carbon sink function consequent to summer desiccation (figure S3(b)). Additionally, dry-adapted *Polytrichum* mosses have become more abundant from absence since then (figures 5(f) and S2). A separately sampled peat core at the same site also has shown an unprecedented,

recent transition of testate amoebae community to dry taxa dominance, but the high-resolution chronology of the transition is not available in that study [106].

Instrumental climate data show no conspicuous long-term trend of regional precipitation, but there are two periods of gradually decreasing precipitation from 1930–1980 CE and 1990–2010 CE that temporally overlap inferred periods of summer desiccation (figures 5(b) and (c)). Therefore, we can reasonably hypothesize that the summer desiccation of *Sphagnum* mosses likely represents a threshold response to a trajectory of intensified surface drying driven by both decreasing precipitation and increasing evapotranspiration under rapid anthropogenic warming at a magnitude of up to 4 °C (figure 5(a)), but the asynchrony still implies that the exact timing of threshold response is likely modulated by local factors. In our case, we find that the late inception of threshold response in HT22-C2 until 1990 CE might be related to a locally wetter condition, as reflected in the relatively higher $\delta^{13}C_{cell}$ values (figure 5(e)), and a lower drainage rate based on the higher AFBD (thus lower hydraulic conductivity [107, 108]) in shallow peat (figure S2). Finally, our isotopic records also document that *Sphagnum* mosses can quickly and successfully recover from summer desiccation after 2010 CE under slightly increased precipitation (figures 5(b), (c) and (e)). This phenomenon may indicate the high sensitivity of *Sphagnum* growth conditions to moisture availability or may provide rare, observational evidence for the resilience of peatlands previously conceptualized in theoretical modeling studies [109–112]. These studies have suggested that peatlands can mitigate drying through self-dampening ecohydrological feedbacks, specifically through complex interactions among water table behaviors, plant production, peat decomposition, and permeability [112].

In summary, our multi-proxy data document profoundly drier conditions associated with dramatic pressures on peatland ecosystems during the CWP. This description differs from some previous studies that simply suggests a weak 'long-term' wetting trend in Northeast China, based on their statistical analysis of national-scale instrumental datasets available only after the 1960s CE [113–115].

### 4.3. Broad implications

The 'drier MWP' and 'wetter LIA' documented in our record align with the climate pattern identified across 'westerlies Asia' but contrast with those in 'monsoonal Asia' (figure 6) [4, 15]. Therefore, our study is important in revealing the dominant role of mid-latitude westerlies, rather than the low-latitude ASM, in propagating continent-scale moisture anomalies to inland Northeast Asia during the pre-industrial era, at a greater distance (>1000 km) than previously recognized. This inference is corroborated by the aforementioned evidence of anti-phased $\delta^{18}O_{precip}$ shifts with 'monsoonal Asia' (figures 4(a) and (b)), challenging the literature that simplistically describes this region as being on the marginal reach of the ASM [32, 34, 116, 117].

The 'drier CWP' documented in our record is also in part consistent with the pattern identified in multiple proxy records across 'westerlies Asia' [118–120]. However, since the 1960s CE, many instrumental records of 'westerlies Asia' indicate a statistically significant trend of increasing precipitation [113], drawing wide interest and discussion about its mechanisms [121, 122], whereas the same wetting trend is quite weak and not statistically significant in inland Northeast Asia (figure 6). In contrast, instrumental records indicate that 'monsoonal Asia' has become drier over the last several decades (figure 6), with proxy records suggesting that this drying trend might persist throughout the CWP, despite being wetter during the MWP [86, 123].

That said, the actual mechanisms driving the spatially opposite moisture anomalies between 'westerlies Asia' and 'monsoonal Asia' as well as the shifting temperature-moisture relationships between natural and anthropogenic climate warming are beyond the scope of this study. These have been previously linked to large-scale ocean–atmosphere systems [15, 124] and responses to different external forcings [86, 125], respectively.

Finally, our study underscores the potential vulnerability of carbon-rich ecosystems over vast inland Northeast Asia not only to ongoing and future climate warming that can exacerbate the impacts of droughts but also to westerlies teleconnection that can spread drought signals widely over the entire Eurasian interior. This remark is in line with an emerging body of recent literature. For example, tree-ring records from Mongolian drylands reveal an abrupt shift beyond a tipping point to widespread soil moisture deficit in the 1990s CE due to enhanced land-atmosphere feedback [20], which may have already left spatially extensive, significant consequences for the function of terrestrial ecosystems. Additionally, warming-induced snowmelt advance and atmospheric circulation reorganization are considered the key drivers for recent widespread extreme forest fire years over northeastern Siberia [126]. Here, we document a complex sequence of responses featuring heterogeneous transitions into plant desiccation, threshold-like behavior, and possible long-term resilience from a moisture-sensitive peatland to multidecadal-scale warming-enhanced drying. These examples all point to both the severity and pervasiveness of anthropogenic climate change impacts on regional terrestrial ecosystems.

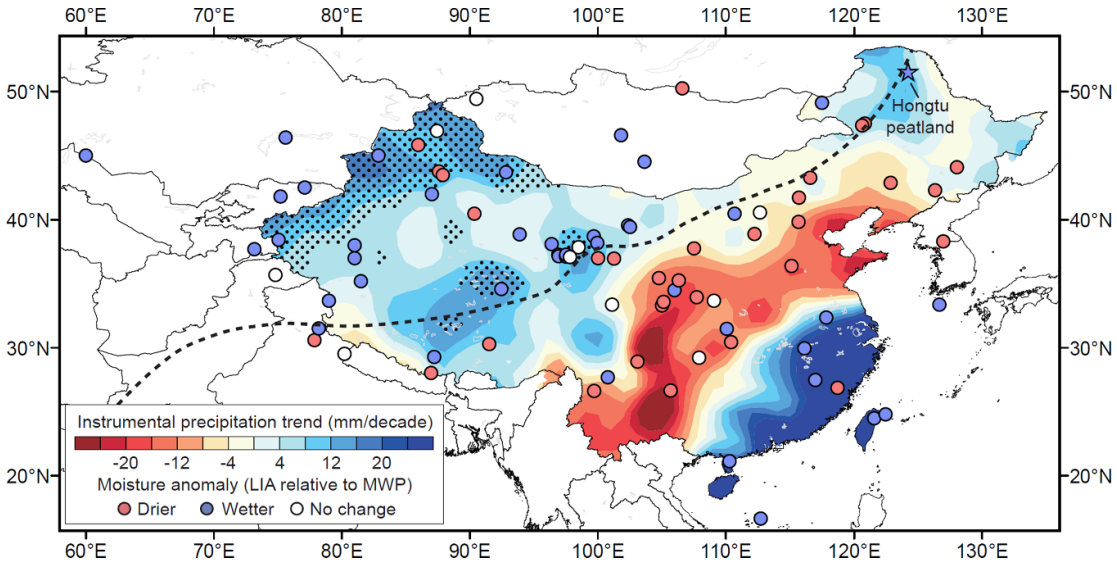


**Figure 6.** Spatial patterns of moisture changes in Asia during the Little Ice Age (LIA) relative to the Medieval Warm Period (MWP) based on the previous paleo-data compilation [4] supplemented with several new sites from Northeast China (table S1) [38, 58, 128–131], and of bias-corrected annual precipitation trend in China during 1961–2016 CE with areas of statistically significant changes stippled (after [113]). The dashed line indicates the modern boundary of the ASM as in [4].

Although significant questions remain regarding the rhythm, spatial extent, magnitude, and carbon-cycle consequences of regional climate change impacts due to a paucity of observational datasets and carbon storage measurements [43, 127], our study demonstrates the value and promise of paleoecological records in providing a long-term context for understanding the trajectory of ecosystem responses to global changes relevant for planning future mitigation and adaptation strategies.

## Data availability statement

All data that support the findings of this study are included within the article (and any supplementary files).

## Acknowledgments

We thank Fengtong Chen, Tingwan Yang and Shuai Zhang for fieldwork assistance, Jingyao Zhao from Xi'an Jiaotong University for sharing speleothem data, and Camille Risi from Université Pierre et Marie Curie for sharing LMDZ4 output. This work was supported by the National Natural Science Foundation of China (42201167 and 42330509), Fundamental Research Funds for the Central Universities (2412023YQ006 and 135112004), National Key R&D Program of China (2023YFF0807200), and Natural Science Foundation of Jilin Province (20230101077JC).

## Conflict of interest

The authors declare no conflict of interest.

## ORCID iD

Zhengyu Xia https://orcid.org/0000-0001-9792-6536

## References

[1] Steinman B A, Stansell N D, Mann M E, Cooke C A, Abbott M B, Vuille M, Bird B W, Lachniet M S and Fernandez A 2022 *Proc. Natl Acad. Sci. USA* **119** e2120015119
[2] Kukla T, Winnick M J, Laguë M M and Xia Z 2023 *Paleoceanogr. Paleoclimatol.* **38** e2022PA004498
[3] Zhang H, Griffiths M L, Chiang J C H, Kong W, Wu S, Atwood A, Huang J, Cheng H, Ning Y and Xie S 2018 *Science* **362** 580–3
[4] Chen F *et al* 2019 *Earth Sci. Rev.* **192** 337–54
[5] Ljungqvist F C, Krusic P J, Sundqvist H S, Zorita E, Brattström G and Frank D 2016 *Nature* **532** 94–98
[6] Woodhouse C A, Meko D M, MacDonald G M, Stahle D W and Cook E R 2010 *Proc. Natl Acad. Sci. USA* **107** 21283–8
[7] Shanahan T M, Overpeck J T, Anchukaitis K J, Beck J W, Cole J E, Dettman D L, Peck J A, Scholz C A and King J W 2009 *Science* **324** 377–80
[8] Fordham D A *et al* 2020 *Science* **369** eabc5654
[9] Nolan C *et al* 2018 *Science* **361** 920–3
[10] Markonis Y, Hanel M, Máca P, Kyselý J and Cook E R 2018 *Nat. Commun.* **9** 1767
[11] Allen K J, Reide F, Gouramanis C, Keenan B, Stoffel M, Hu A and Ionita M 2022 *Environ. Res. Lett.* **17** 055011
[12] Shepherd T G 2014 *Nat. Geosci.* **7** 703–8
[13] Greve P, Orlowsky B, Mueller B, Sheffield J, Reichstein M and Seneviratne S I 2014 *Nat. Geosci.* **7** 716–21
[14] Milly P C D and Dunne K A 2016 *Nat. Clim. Change* **6** 946–9
[15] Chen J, Chen F, Feng S, Huang W, Liu J and Zhou A 2015 *Quat. Sci. Rev.* **107** 98–111
[16] Chen F *et al* 2008 *Quat. Sci. Rev.* **27** 351–64
[17] Herzschuh U *et al* 2019 *Nat. Commun.* **10** 2376
[18] Lu J, Yang H, Griffiths M L, Burls N J, Xiao G, Yang J, Wang J K, Johnson K R and Xie S 2021 *Earth Planet. Sci. Lett.* **563** 116882

[19] Chen A *et al* 2024 *Palaeogeogr. Palaeoclimatol. Palaeoecol.* **650** 112352
[20] Zhang P, Jeong J-H, Yoon J-H, Kim H, Wang S-Y S, Linderholm H W, Fang K, Wu X and Chen D 2020 *Science* **370** 1095–9
[21] Hessl A E, Anchukaitis K J, Jelsema C, Cook B, Byambasuren O, Leland C, Nachin B, Pederson N, Tian H and Hayles L A 2018 *Sci. Adv.* **4** e1701832
[22] Wang X, Brown P M, Zhang Y, Song L and Añel J A 2011 *PLoS One* **6** e22740
[23] Zhang T, Yuan Y, Wei W, Yu S, Zhang R, Chen F, Shang H and Qin L 2014 *Quat. Res.* **82** 14–21
[24] Davi N, Jacoby G, Fang K, Li J, D'Arrigo R, Baatarbileg N and Robinson D 2010 *J. Geophys. Res. Atmos.* **115** D22103
[25] Shi Z *et al* 2016 *J. Plant Ecol.* **9** 51–60
[26] Zhao J *et al* 2021 *Quat. Sci. Rev.* **254** 106793
[27] Zhang X, Jin L, Lu H, Park W, Schneider B and Latif M 2018 *Glob. Planet. Change* **170** 190–200
[28] Zheng Y, Pancost R D, Naafs B D A, Li Q, Liu Z and Yang H 2018 *Earth Planet. Sci. Lett.* **493** 36–46
[29] Zhang M, Bu Z, Wang S and Jiang M 2020 *Earth Sci. Rev.* **201** 102984
[30] Chu G, Sun Q, Wang X, Li D, Rioual P, Qiang L, Han J and Liu J 2009 *J. Geophys. Res. Atmos.* **114** D22108
[31] Han D, Gao C, Yu Z, Yu X, Li Y, Cong J and Wang G 2019 *Quat. Int.* **532** 138–45
[32] Gao C, He J, Zhang Y, Cong J, Han D and Wang G 2018 *Glob. Planet. Change* **162** 313–20
[33] Yu S-H, Zheng Z, Kershaw P, Skrypnikova M and Huang K-Y 2017 *Quat. Int.* **432** 79–92
[34] Zhou X *et al* 2016 *Earth Planet. Sci. Lett.* **456** 39–46
[35] FAO 2021 *Map of Aridity (Global—∼19km)* (AQUASTAT FAO-UN Land and Water Division)
[36] Hugelius G *et al* 2020 *Proc. Natl Acad. Sci. USA* **117** 20438–46
[37] Brown J, Ferrians O, Heginbottom J A and Melnikov E 2002 *Circum-Arctic Map of Permafrost and Ground-ice Conditions Version 2* (National Snow and Ice Data Center)
[38] Wen R, Xiao J, Chang Z, Zhai D, Xu Q, Li Y and Itoh S 2010 *Boreas* **39** 262–72
[39] Liu X, Zhang X, Zhao L, Xu G, Wang L, Sun W, Zhang Q, Wang W, Zeng X and Wu G 2017 *J. Geophys. Res. Atmos.* **122** 6697–712
[40] Gu C and Zhai W 2019 *Econ. Geogr.* **39** 8–20 (in Chinese with an English abstract)
[41] Santoro M *et al* 2021 *Earth Syst. Sci. Data* **13** 3927–50
[42] Krawchuk M A, Moritz M A, Parisien M-A, Van Dorn J, Hayhoe K and Chave J 2009 *PLoS One* **4** e5102
[43] Fan L *et al* 2023 *Nat. Geosci.* **16** 56–62
[44] Jin H, Li S, Cheng G, Shaoling W and Li X 2000 *Glob. Planet. Change* **26** 387–404
[45] Huang J, Yu H, Guan X, Wang G and Guo R 2016 *Nat. Clim. Change* **6** 166–71
[46] Yao J, Liu H, Huang J, Gao Z, Wang G, Li D, Yu H and Chen X 2020 *Nat. Commun.* **11** 1665
[47] Li Q *et al* 2024 *Land Degrad. Dev.* **35** 1863–73
[48] Denissen J M C, Teuling A J, Pitman A J, Koirala S, Migliavacca M, Li W, Reichstein M, Winkler A J, Zhan C and Orth R 2022 *Nat. Clim. Change* **12** 677–84
[49] Jin H, Yu Q, Lü L, Guo D, He R, Yu S, Sun G and Li Y 2007 *Permafr. Periglac. Process.* **18** 245–58
[50] Lang H-Q 1981 *Acta Bot. Sin.* **23** 470–7 (in Chinese with English abstract)
[51] Vitt D H, Bayley S E and Jin T-L 1995 *Can. J. Fish. Aquat. Sci.* **52** 587–606
[52] Bowen G J, Wassenaar L I and Hobson K A 2005 *Oecologia* **143** 337–48
[53] Risi C, Bony S, Vimeux F and Jouzel J 2010 *J. Geophys. Res.* **115** D12118
[54] Yoshimura K, Kanamitsu M, Noone D and Oki T 2008 *J. Geophys. Res. Atmos.* **113** D19108
[55] Blaauw M and Christen J A 2011 *Bayesian Anal.* **6** 457–74
[56] Chambers F M, Beilman D W and Yu Z 2010 *Mires Peat* **7** 7
[57] Yu Z, Campbell I D, Campbell C, Vitt D H, Bond G C and Apps M J 2003 *Holocene* **13** 801–8
[58] Xia Y, Yang Z, Sun J, Xia Z and Yu Z 2024 *Quat. Sci. Rev.* **324** 108466
[59] Yu Z, Vitt D H, Campbell I D and Apps M J 2003 *Can. J. Bot.* **81** 267–82
[60] Cai S and Yu Z 2011 *Quat. Res.* **75** 531–40
[61] Mauquoy D, Hughes P D M and Geel B V 2010 *Mires Peat* **7** 6
[62] Mauquoy D and Barber K 1999 *J. Quat. Sci.* **14** 263–75
[63] Hughes P D M and Barber K E 2004 *Holocene* **14** 65–77
[64] Treat C C *et al* 2016 *J. Geophys. Res. Biogeosci.* **121** 78–94
[65] Barber K E, Chambers F M and Maddy D 2003 *Quat. Sci. Rev.* **22** 521–39
[66] Yang Q, Li H, Zhao H, Chambers F M, Bu Z, Bai E and Xu G 2022 *CATENA* **216** 106412
[67] Xia Z, Yu Z and Loisel J 2018 *Geology* **46** 855–8
[68] Kaislahti Tillman P, Holzkämper S, Kuhry P, Sannel A B K, Loader N J and Robertson I 2010 *Chem. Geol.* **270** 216–26
[69] Loader N J, Robertson I, Barker A C, Switsur V R and Waterhouse J S 1997 *Chem. Geol.* **136** 313–7
[70] Xia Z, Zheng Y, Stelling J M, Loisel J, Huang Y and Yu Z 2020 *Geochim. Cosmochim. Acta* **277** 265–84
[71] Loisel J, Garneau M and Hélie J-F 2010 *Holocene* **20** 285–91
[72] Lamentowicz M, Cedro A, Gałka M, Goslar T, Miotk-Szpiganowicz G, Mitchell E A D and Pawlyta J 2008 *Palaeogeogr. Palaeoclimatol. Palaeoecol.* **265** 93–106
[73] Daley T J, Barber K E, Street-Perrott F A, Loader N J, Marshall J D, Crowley S F and Fisher E H 2010 *Quat. Sci. Rev.* **29** 1590–601
[74] Turetsky M R, Manning S W and Wieder R K 2004 *Wetlands* **24** 324–56
[75] Clymo R S 1984 *Phil. Trans. R. Soc.* B **303** 368–88
[76] Yu Z, Turetsky M R, Campbell I D and Vitt D H 2001 *Ecol. Model.* **145** 159–73
[77] Young D M, Baird A J, Charman D J, Evans C D, Gallego-Sala A V, Gill P J, Hughes P D M, Morris P J and Swindles G T 2019 *Sci. Rep.* **9** 17939
[78] Piilo S R, Zhang H, Garneau M, Gallego-Sala A, Amesbury M J and Väliranta M M 2019 *Environ. Res. Lett.* **14** 075002
[79] Konecky B L *et al* 2023 *Nat. Geosci.* **16** 997–1004
[80] Leuenberger M 2007 *Stable Isotopes as Indicators of Ecological Change* vol 1, ed T E Dawson and R T W Siegwolf (Elsevier) pp 211–33
[81] Zhang X-M, Chen L, Ji J-Z, Wang J, Wang Y-B, Guo W and Lan B-W 2011 *J. Meteorol. Environ.* **27** 13–20 (in Chinese with an English abstract)
[82] Loader N J *et al* 2016 *J. Quat. Sci.* **31** 426–35
[83] Williams T G and Flanagan L B 1996 *Oecologia* **108** 38–46
[84] Loisel J, Garneau M and Hélie J-F 2009 *J. Quat. Sci.* **24** 209–14
[85] Ge Q, Zheng J, Hao Z and Liu H 2013 *Sci. China Earth Sci.* **56** 321–9
[86] Liu J, Rühland K M, Chen J, Xu Y, Chen S, Chen Q, Huang W, Xu Q, Chen F and Smol J P 2017 *Nat. Clim. Change* **7** 190–4
[87] Loisel J, Sarna K, Xia Z, Huang Y and Yu Z 2023 *Geology* **51** 247–51
[88] Granath G *et al* 2018 *Biogeosciences* **15** 5189–202
[89] Xia Z and Yu Z 2020 *Front. Earth Sci.* **8** 307
[90] Sternberg L D S L, Deniro M J and Savidge R A 1986 *Plant Physiol.* **82** 423–7
[91] Bowen G J 2008 *J. Geophys. Res. Atmos.* **113** D05113
[92] Zhang P *et al* 2008 *Science* **322** 940–2
[93] Liu Z *et al* 2014 *Quat. Sci. Rev.* **83** 115–28
[94] Wang Y, Cheng H, Edwards R L, He Y, Kong X, An Z, Wu J, Kelly M J, Dykoski C A and Li X 2005 *Science* **308** 854–7
[95] Zhang J, Chen F, Holmes J A, Li H, Guo X, Wang J, Li S, Lü Y, Zhao Y and Qiang M 2011 *Quat. Sci. Rev.* **30** 1973–87
[96] Cleary K G, Xia Z and Yu Z 2024 *J. Geophys. Res. Biogeosci.* **129** e2023JG007890

[97] Schipperges B and Rydin H 1998 *New Phytol.* **140** 677–84
[98] McNeil P and Waddington J M 2003 *J. Appl. Ecol.* **40** 354–67
[99] Küttim M, Küttim L, Ilomets M and Laine A M 2020 *Ecol. Res.* **35** 219–34
[100] Laine A M, Juurola E, Hájek T and Tuittila E-S 2011 *Oecologia* **167** 1115–25
[101] Loisel J, Gallego-Sala A V and Yu Z 2012 *Biogeosciences* **9** 2737–46
[102] Moore T R, Bubier J L, Frolking S E, Lafleur P M and Roulet N T 2002 *J. Ecol.* **90** 25–36
[103] Asada T, Warner B G and Banner A 2003 *Bryologist* **106** 516–27
[104] Moore T R 1989 *Can. J. Bot.* **67** 1203–7
[105] Brock T C M and Bregman R 1989 *Oecologia* **80** 44–52
[106] Li X, Han D, Cong J, Gao C and Wang G 2024 *Atmosphere* **15** 314
[107] Morris P J, Baird A J, Eades P A and Surridge B W J 2019 *Water Resour. Res.* **55** 1531–43
[108] Morris P J *et al* 2022 *Water Resour. Res.* **58** e2022WR033181
[109] Morris P J, Baird A J, Young D M and Swindles G T 2015 *Geophys. Res. Lett.* **42** 10788–97
[110] Waddington J M, Morris P J, Kettridge N, Granath G, Thompson D K and Moore P A 2015 *Ecohydrology* **8** 113–27
[111] Page S E and Baird A J 2016 *Annu. Rev. Environ. Resour.* **41** 35–57
[112] Morris P J, Belyea L R and Baird A J 2011 *J. Ecol.* **99** 1190–201
[113] Zhang Y, Ren Y, Ren G and Wang G 2020 *J. Geophys. Res. Atmos.* **125** e2019JD031728
[114] Li W and Chen Y 2021 *Int. J. Climatol.* **41** E1980–91
[115] Zhang X, Liu X, Wang W, Zhang T, Zeng X, Xu G, Wu G and Kang H 2018 *Hydrol. Process.* **32** 1449–60
[116] Sun L, Shen B, Sui B and Huang B 2017 *Clim. Dyn.* **48** 1647–59
[117] Liu R, Liu Y, Li Q, Song H, Li X, Sun C, Cai Q and Song Y 2019 *Clim. Dyn.* **53** 3661–74
[118] Chen F, Huang X, Zhang J, Holmes J A and Chen J 2006 *Sci. China* D **49** 1280–90
[119] Wang Z 1992 *Chin. Geogr. Sci.* **2** 215–25
[120] Chen J, Liu J, Zhang X, Chen S, Huang W, Chen J, Zhang S, Zhou A and Chen F 2019 *Clim. Dyn.* **53** 1517–26
[121] Chen F, Xie T, Yang Y, Chen S, Chen F, Huang W and Chen J 2023 *Sci. China Earth Sci.* **66** 1241–57
[122] Shi Y, Shen Y, Kang E, Li D, Ding Y, Zhang G and Hu R 2007 *Clim. Change* **80** 379–93
[123] Lan J *et al* 2020 *Geology* **48** 307–12
[124] Cook E R, Anchukaitis K J, Buckley B M, D'Arrigo R D, Jacoby G C and Wright W E 2010 *Science* **328** 486–9
[125] Liu J, Wang B, Cane M A, Yim S-Y and Lee J-Y 2013 *Nature* **493** 656–9
[126] Scholten R C, Coumou D, Luo F and Veraverbeke S 2022 *Science* **378** 1005–9
[127] Tang H, Li Z, Zhu Z, Chen B, Zhang B and Xin X 2015 *Remote Sens.* **7** 11914–32
[128] Fu Y, Li Y and Yu Z 2022 *Quat. Sci. Rev.* **295** 107781
[129] Lv F, Sun Y, Wang X and Zhang P 2024 *Palaeogeogr. Palaeoclimatol. Palaeoecol.* **640** 112089
[130] Mao X, Wan D, Song L, Yang J, Liu L, Jiang G, Li J and Liu X 2021 *J. Paleolimnol.* **66** 103–16
[131] Lin Q, Leng X and Hong B 2004 *Bull. Minerel. Pet. Geol.* **23** 15–18 (in Chinese with English abstract)